A high-resolution geochemical record from the Kuche depression: Constraints on early Miocene uplift of South...

Article *in* Palaeogeography Palaeoclimatology Palaeoecology · March 2016

DOI: 10.1016/j.palaeo.2016.01.020

CITATIONS
0

READS
169

6 authors, including:

Zihua Tang
Chinese Academy of Sciences
18 PUBLICATIONS **146** CITATIONS
SEE PROFILE

Shiling Yang
Chinese Academy of Sciences
48 PUBLICATIONS **2,235** CITATIONS
SEE PROFILE

Qingqing Qiao
Chinese Academy of Sciences
17 PUBLICATIONS **223** CITATIONS
SEE PROFILE

Baochun Huang
Peking University
92 PUBLICATIONS **2,410** CITATIONS
SEE PROFILE

Palaeogeography, Palaeoclimatology, Palaeoecology 446 (2016) 1–10

Contents lists available at ScienceDirect

Palaeogeography, Palaeoclimatology, Palaeoecology

journal homepage: www.elsevier.com/locate/palaeo

A high-resolution geochemical record from the Kuche depression: Constraints on early Miocene uplift of South Tian Shan

Zihua Tang [a,b,*], Shiling Yang [a], Qingqing Qiao [c], Feng Yin [d], Baochun Huang [e], Zhongli Ding [a]

[a] Key Laboratory of Cenozoic Geology and Environment, Institute of Geology and Geophysics, Chinese Academy of Sciences, Beijing 100029, China
[b] CAS Center for Excellence in Tibetan Plateau Earth Sciences, China
[c] Xinjiang Research Center for Mineral Resources, Xinjiang Institute of Ecology and Geography, Chinese Academy of Sciences, Urumqi 830011, China
[d] China University of Geoscience, Beijing 100083, China
[e] Key Laboratory of Orogenic Belt of Crustal Evolution Ministry of Education, School of Earth and Space Sciences, Peking University, Beijing 100871, China

ARTICLE INFO

Article history:
Received 2 August 2015
Received in revised form 5 December 2015
Accepted 8 January 2016
Available online xxxx

Keywords:
Mountain uplift
Tian Shan
Cenozoic
Major elements
Kuche depression

ABSTRACT

The building of Tian Shan is often simplified to a Cenozoic reactivation of a Paleozoic fold belt. During the past decades extensive case studies have arrived at the conclusion that Tian Shan experienced diachronous uplift during the Cenozoic, however, understanding of the specific location and duration of the mountain building is still hindered by complex tectonic history of the orogenic belt. Considering the geochemical differences of various tectonic units within the mountains, we studied the chemical composition variability for the carbonate-free fine-grained samples collected from the longest terrestrial outcrop in the Kuche depression, southern Tian Shan, at a high resolution in order to better constrain the orogenic process. Our data show significant increases in mobile elements during the interval of 23–17 Ma, departing substantially from the stable long-term weathering trends and limited sedimentary sorting effects. We interpret the trend as provenance changes, which provide crucial evidence to support that the South Tian Shan experienced significant surface uplift during the early Miocene. This argument is supported by other studies conducted on both local and regional scales. Mineralogical analyses for the study section have shown that, since the early Neogene, a marked increase of detrital limeclasts derived from the South Tian Shan is accompanied by the decreases of the abundance of garnets derived from an ultrahigh-pressure metamorphic fold belt in the central Tian Shan. Moreover, low-temperature thermochronological results revealed that the central Tian Shan merely experienced pre-Neogene cooling, contrasting to the southern piedmont of the mountain where Neogene cooling dominated. Taken all together, we conclude that the uplift of the South Tian Shan initiated at ~23 Ma and the paleoelevation may exceed the height of the central Tian Shan at ~17 Ma.

1. Introduction

With peaks higher than 7000 m, the Tian Shan Mountains dominate Central Eurasian landscape over an E–W distance of 2500 km. The tectonic history of the mountains may be tracked to Paleozoic, when the region was deformed into a fold belt (Windley et al., 1990; Xiao et al., 2015). The mountains are sandwiched by the Junggar and the Tarim basins throughout the Meso- and Cenozoic eras (Hendrix et al., 1992; Windley et al., 1990) and shed thick clastic sediments on its flanks. The present Tian Shan is predominately a product of tectonic rejuvenation in response to the India–Asia collision during the Cenozoic (Avouac et al., 1993; Molnar and Tapponnier, 1975; Yin et al., 1998).

Although the tectonic process that formed the Tian Shan has been extensively studied, the precise timing and duration of the building of the present Tian Shan are still open to debate. By applying modern shortening rate across the Tian Shan, a middle Miocene (Abdrakhmatov et al., 1996; Artyushkov and Hofmann, 1998), which roughly agrees with those ages derived from mass balance calculation between the Tian Shan and its adjacent basins (Métivier and Gaudemer, 1997). These arguments, however, are undermined by poor chronological constraints, the assumption that shortening rate did not change for ~15 Ma, and the basin fill were precisely dated. Low temperature thermochronology studies suggest that the onset of exhumation varies from the late Oligocene (Dumitru et al., 2001; Heermance et al., 2007; Hendrix et al., 1994; Macaulay et al., 2014) to the middle to late Miocene (Bullen et al., 2001, 2003; Sobel et al., 2006) at different parts of the mountains.

Within improved chronostratigraphic framework based on high-resolution magnetostratigraphy, the onset of growth strata, the timing of initiation of coarse clastic sedimentation, and the increase in

* Corresponding author at: Key Laboratory of Cenozoic Geology and Environment, Institute of Geology and Geophysics, Chinese Academy of Sciences, Beijing 100029, China. Tel.: +86 10 8299 8301; fax: +86 10 6201 0846.
E-mail addresses: tangzihua@mail.iggcas.ac.cn, tangzihua@yahoo.com (Z. Tang).

http://dx.doi.org/10.1016/j.palaeo.2016.01.020
0031-0182/

sedimentation rates in sedimentary basins can represent the minimum ages of the onset of the deformation in the Tian Shan. Results from various locations within the Tian Shan generally show that deformation occurred during four time intervals: early Miocene (25–20 Ma, e.g., Heermance et al., 2008; Huang et al., 2006; Tang et al., 2012; Wack et al., 2014; Yang et al., 2015; Yin et al., 1998), middle Miocene (17–15 Ma, e.g. Charreau et al., 2009a; Heermance et al., 2007, 2008; Huang et al., 2006; Tang et al., 2012), early late Miocene (11–10 Ma, e.g. Bullen et al., 2001; Charreau et al., 2005; Charreau et al., 2006; Charreau et al., 2009b; Wack et al., 2014), and latest Miocene (7–5 Ma; e.g. Jing et al., 2011; Li et al., 2010; Sun et al., 2009; Sun and Zhang, 2009). Taking into account the heterogeneous mountain building and complex tectonic history of the orogenic belt, such observations have poor constraints on the specific location and duration of the deformed region.

The Kezilenuer section in the Kuche depression is the longest known fluviolacustrine sequence within the southern Tian Shan (Huang et al., 2006; Li et al., 2006b). The section spans from the late Paleogene throughout the Miocene. We here assess previous magnetostratigraphic correlations by using a statistical method and present chemical compositions of bulk fined-grained rock samples collected from the section. By combining these data with previously published low-resolution data of detrital mode and mineral composition, we aim at constraining the exhumation histories and determining the location and duration of the mountain building of the southern Tian Shan.

2. Geological setting

The Tian Shan orogenic belt consists of microcontinental blocks containing Precambrian basements and Meso-Cenozoic depositional covers. In the southwestern Chinese Tian Shan, the Tarim plate and the Central Tian Shan plate were assembled during the early Carboniferous, resulting in widespread ultrahigh-pressure eclogite and blueschists along the Southern Central Tian Shan Suture (SCTS, Han et al., 2011, Fig. 1a). To the south of the suture deformed Paleozoic carbonate shelf is well exposed, on the Harke Mountain, which is the summit of the present South Tian Shan. The Paleozoic sedimentary rocks mainly consist of Silurian to Carboniferous limestone, marble, flysche, chert and clastic sedimentary rocks (Fig. 1b & c).

The Kuche depression is a foreland basin resulting from southward thrusting of the South Tian Shan (Yin et al., 1998). It extends 300–400 km west to east with a width of 40–70 km, occupying ca.

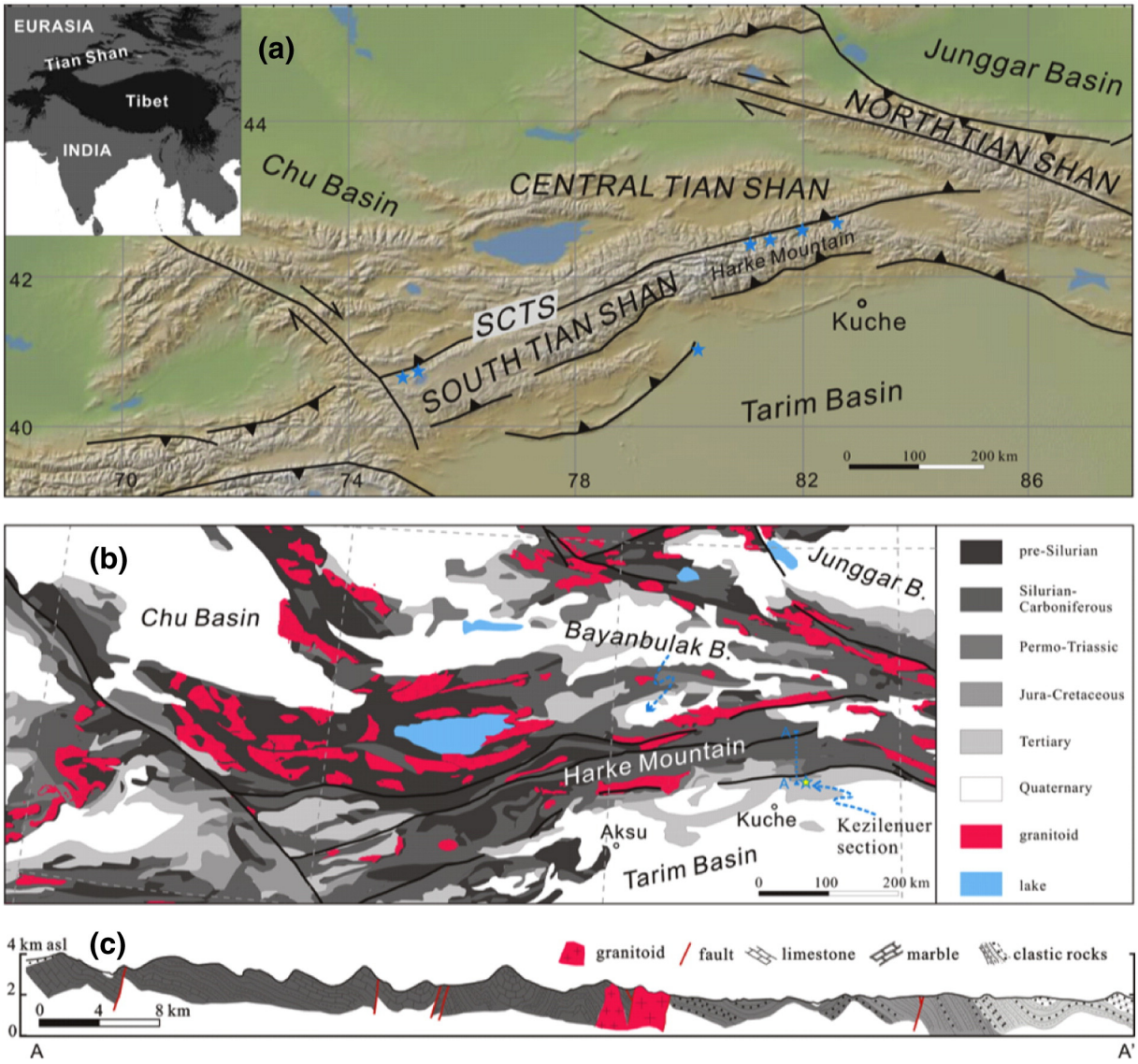

Fig. 1. (a) Topographic map of the Tian Shan with main faults that divide the mountain into North, Central and South Tian Shan. SCTS represents the Southern Central Tian Shan Suture and the blue stars indicate the sites of UHP metamorphic rocks (Han et al., 2011); (b) simplified geological map of the study area, showing the location of the study section. Note the transection A–A′; (c) transection A–A′ in (b). (For interpretation of the references to color in this figure legend, the reader is referred to the web version of this article.)

2.8×10^4 km^2. The Kuche depression accumulated about 10 km of sediments shed from the Tian Shan throughout the Mesozoic and Cenozoic, of which 5–6 km are assigned to the Cenozoic. Between the late Cretaceous and the early Cenozoic the western part of the depression was intermittently influenced by a series of shallow marine transgressions (Hao et al., 2000).

The Cenozoic strata overlie the Cretaceous strata unconformably and, in ascending order, comprise the Kumugeliemu Group, and the Suweiyi, Jidike, Kangcun, Kuche and Xiyu formations without significant hiatus between them. The Kumugeliemu Group contains two distinct sedimentary facies (Li, 1984). In the western part of the basin the group mainly consists of intercalated sandstone and shale deposits in lagoon environments and evaporites deposited in close lake environments, while in the eastern part of the basin the group contains silicilastic sedimentary rocks deposited in fluvial and lacustrine environments, and the grain size becomes finer southward. The formations overlying the Kumugeliemu Group are widely distributed in the linear folds of the Kuche depression and comprise interbedded conglomerate, sandstone and siltstone, and the frequency of conglomerate increases upward.

3. Chronology revisited

Based on poorly preserved marine fossil assemblages from the western Kuche depression, the age of lower Kumugeliemu Group was assigned to be the late Paleogene and the early Eocene (Su et al., 2003; Zhu et al., 2012). Because of the spatial variations of sedimentary facies (Li, 1984; Zhou et al., 2001) and the diachroneity of marine regression (e.g. Bosboom et al., 2014; Sun and Jiang, 2013), it is unreliable to correlate the group in the eastern part of the basin directly to that of the western part of the depression.

As one of the type sections for the Cenozoic sedimentary rocks in the Kuche depression, the Kezilenuer section (83°17.5′E, 42°02.4′E) exposes thick, continuous deposits ranging from the Kumugeliemu Group to the Xiyu Formation (Li et al., 2006b). Due to the absence of characteristic fossils used for age control and the ashed beds used for isotopic dating, magnetostratigraphy might be the most powerful approach to date the section. Huang and colleagues conducted detailed magnetostratigraphic analyses for the section and established a high-resolution magnetic polarity sequence based on 969 samples (Huang et al., 2006). Basically based on the observed distinctive and well-established magnetozones, they suggested that the Kezilenuer section was deposited from magnetostratigraphic Chron C11n.1n to C3r of the geomagnetic polarity time scale (GPTS), i.e. between 29.183 and 6.033 Ma following the latest GPTS (Ogg, 2012). This section is the longest terrestrial section in the southern Tian Shan, playing a crucial role for understanding regional tectonic deformation during the Cenozoic.

Zhang et al. (2014) adopted Huang's original correlation for the upper part of the section and stretched the lower part to ca. 40 Ma, yielding a basal age ~10 Ma older than the original argument. With the reinterpreted chronology they suggest that the South Tian Shan experienced accelerated shortening since the late Eocene.

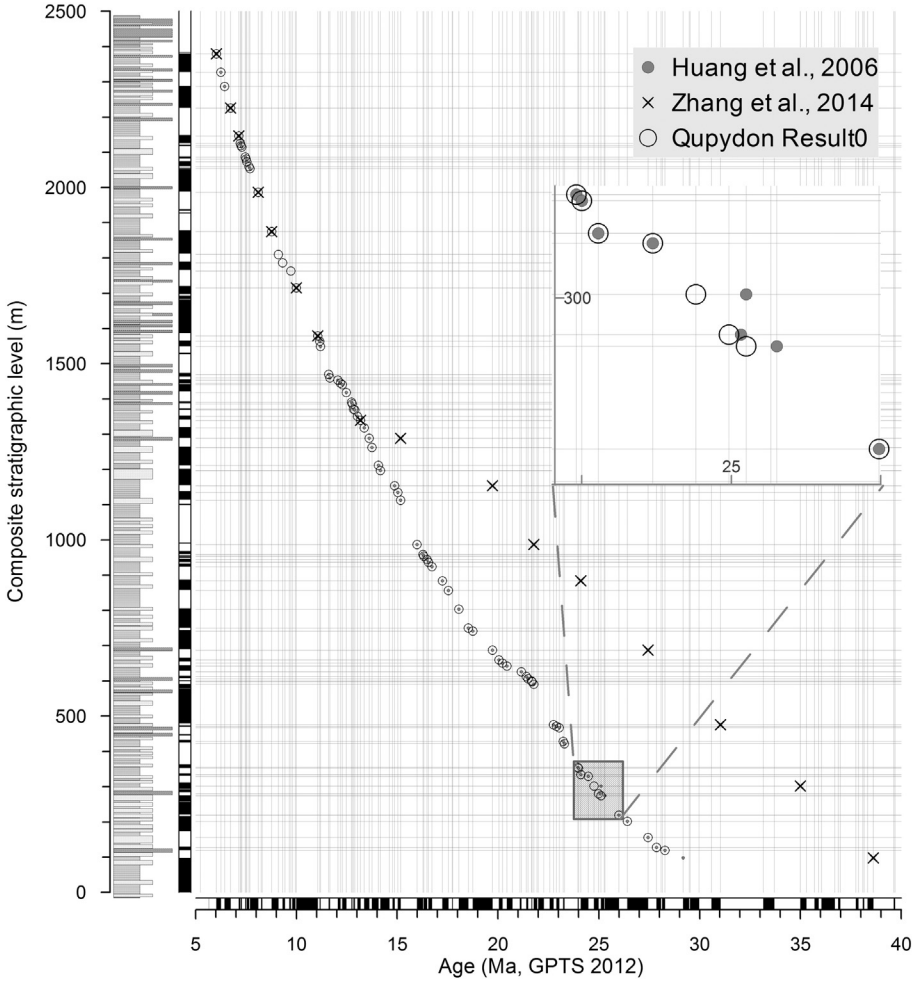

Fig. 2. Magnetostratigraphy for the Kezilenuer section showing different correlations to the GPTS (Ogg, 2012), proposed by Huang et al. (2006), Zhang et al. (2014), and the dynamic time warping algorithm (Lallier et al., 2013). The enlarged inset indicates the differences between the correlations by Huang et al. (2006) and by the algorithm presented in the study (Qupydon Result0).

Admittedly, without robust constraints from radiometric ages and diagnostic fossils, visually magnetostratigraphic correlation is somewhat a subjective practice. Nevertheless, statistical tests can improve the quality and reduce the uncertainty of a correlation. Here we correlate the observed polarity sequence with the GPTS (Ogg, 2012) based on the dynamic time warping algorithm (Lallier et al., 2013). With an assumption of locally stationary sedimentation rates, the algorithm induces the correlation cost, which is designed to measure the local variations of the accumulation rate within the predicted chronological framework, and finds the minimum correlation cost. We calculated the correlation costs for 5000 potential correlations using the program Qupydon within the C-sequence of the GPTS. As a result, 50 minimum cost outputs unanimously correlate the sequence to the magnetostratigraphic Chron C10r to C3An.1n, and the differences among them are trivial. The 50 correlations and their costs can be found in the Supplementary materials.

We here adopt the least cost correlation (Rank 0) recommended by the algorithm and compare it with the framework proposed by Huang et al. (2006) and Zhang et al. (2014) through an age-thickness plot (Fig. 2). The statistically least cost correlation (i.e. the best correlation) bears a striking similarity to the original chronology proposed by Huang et al. (2006) with negligible differnce around 25 Ma. In contrast, the re-interpreted chronology for the lower part of the section (Zhang et al., 2014) is deviated from these solutions. According to their reinterpretation, the observed magnetic polarity sequence has more than 50% chrons missed or unidentified, which is unacceptable for reliable magnetostratigraphic correlation. Furthermore, the reinterpretation predicts a sedimentation rate of ~5 cm/ka for the lower part of the section, which is extraordinarily low relative to any previous data from the surroundings (e.g. Charreau et al., 2006; Sun et al., 2009; Tang et al., 2011; Lu et al., 2014).

Our statistical assessment validates the original magnetostratigraphic chronology determined by Huang et al. (2006).

4. Chemical composition analysis

4.1. Material and methods

In this study we analyzed the chemical composition of 190 bulk samples collected from the Kezilenuer section, yielding an average sampling interval of ~12.5 m (55–180 ka). Most samples came from mudstone and siltstone in the fluviolacustrine deposits and no samples were taken from conglomeratic units.

These samples were finely ground in an agate mortar and treated with 1 M acetic acid to remove carbonate. The acid-insoluble residue was rinsed four times with deionized water and evaporated to dryness in an oven at 105 °C. About 0.5 g of carbonate-free sample was heated to 1000 °C in a muffle furnace to determine the loss on ignition (LOI), and then mixed with 6 g of $Li_2B_4O_7$ and fused to a glass bead in a platinum crucible. The prepared beads were measured on a Shimadzu XRF-1500 for abundances of major elements in the Institute of Geology and Geophysics, CAS. The reproducibility of element measurements, tested by replicate analyses of the IGGE reference sample GSS-5, is better than 5% for all major oxides. The reproducibility of P_2O_5 and MnO is 10%.

Weight percentages of the oxides of major elements produced by XRF were recalculated to molar ratios for evaluating chemical weathering condition. Moreover, we employed a linear least squares regression to estimate the long-term geochemical trend of the study section and conducted *t*-test to evaluate the significance of the linear trend.

4.2. Results

Weight percentages of major oxides from the Kezilenuer section are presented in Fig. 3. The carbonate-free samples consist mainly of SiO_2, Al_2O_3, Fe_2O_3, K_2O, and MgO, with low concentrations of Na_2O, TiO_2, CaO, and MnO. The abundances of major elements generally display

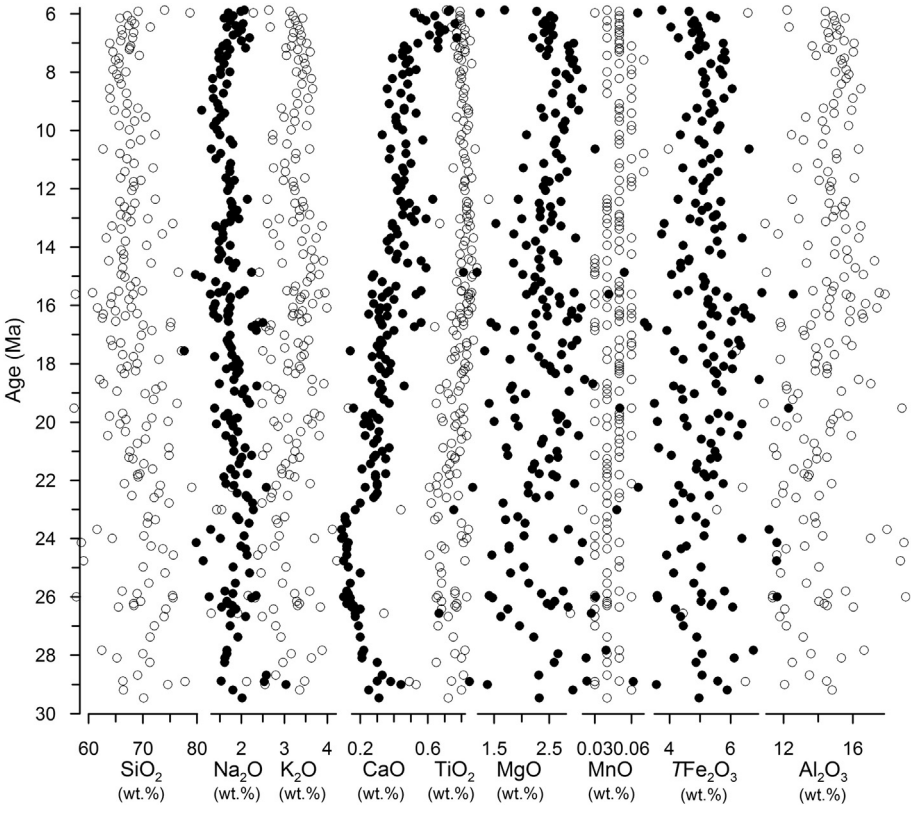

Fig. 3. Abundance of major oxides for carbonate-free samples collected from the study section as a function of age.

smaller variation in the upper section compared to the lower section. For example, Al_2O_3 abundance has standard deviations of 2.18 and 1.38 prior to and after 15 Ma, respectively.

The overall trends of the relative concentrations of SiO_2 and Na_2O are similar. They exhibit statistically significant but poorly defined decreases upward ($n = 190$, $p < 0.001$) until ~7 Ma, and slight increases upward after ~7 Ma. The relative concentrations of Al_2O_3 and CaO show stepwise increases. The relative concentration of Al_2O_3 increases at ~15 Ma and the relative concentration of CaO increases at ~23 and ~7 Ma. The rest of Fe_2O_3, K_2O, TiO_2, and MnO, show relatively stable concentrations throughout the sequence.

5. Discussion

Factors influencing bulk geochemistry of clastic sediments chiefly include: (1) weathering intensity, (2) sedimentary sorting, and (3) provenance (Nesbitt, 2003). Major elements greatly differ in their susceptibilities to fractionation during weathering and transport, allowing us to deduce the information of alteration and sorting history from sedimentary geochemistry.

5.1. Testing element immobility

Major element composition of fine-grained sediments, reflecting their primary mineralogy, is sensitive to the modifications during transportation and weathering. According to their abundances in the dissolved load of rivers worldwide, elements are primarily ranked by their mobility (Gaillardet et al., 2003). Among the major elements, magnesium (Mg), sodium (Na), and calcium (Ca) fall into the highly mobile group, potassium (K) and manganese (Mn) to moderately mobile group, on the other hand, iron (Fe), titanium (Ti), and aluminum (Al) pertain to the immobile group.

As mobile elements are lost from, or gained by, the rock, immobile elements will increase or decrease in abundances (Argast and Donnelly, 1987; Gresens, 1967). Element immobility can thus be further tested using bivariate plots. If both Al_2O_3 and TiO_2 were immobile, the concentrations of their oxides should form a line extending to the origin when they are plotted against each other (Christidis, 1998; MacLean, 1990). Furthermore, immobile-SiO_2 element plots should show linear arrangements of data points, intercepting at 100% SiO_2 for the immobile elements concentrated in clay fractions or 0% SiO_2 for

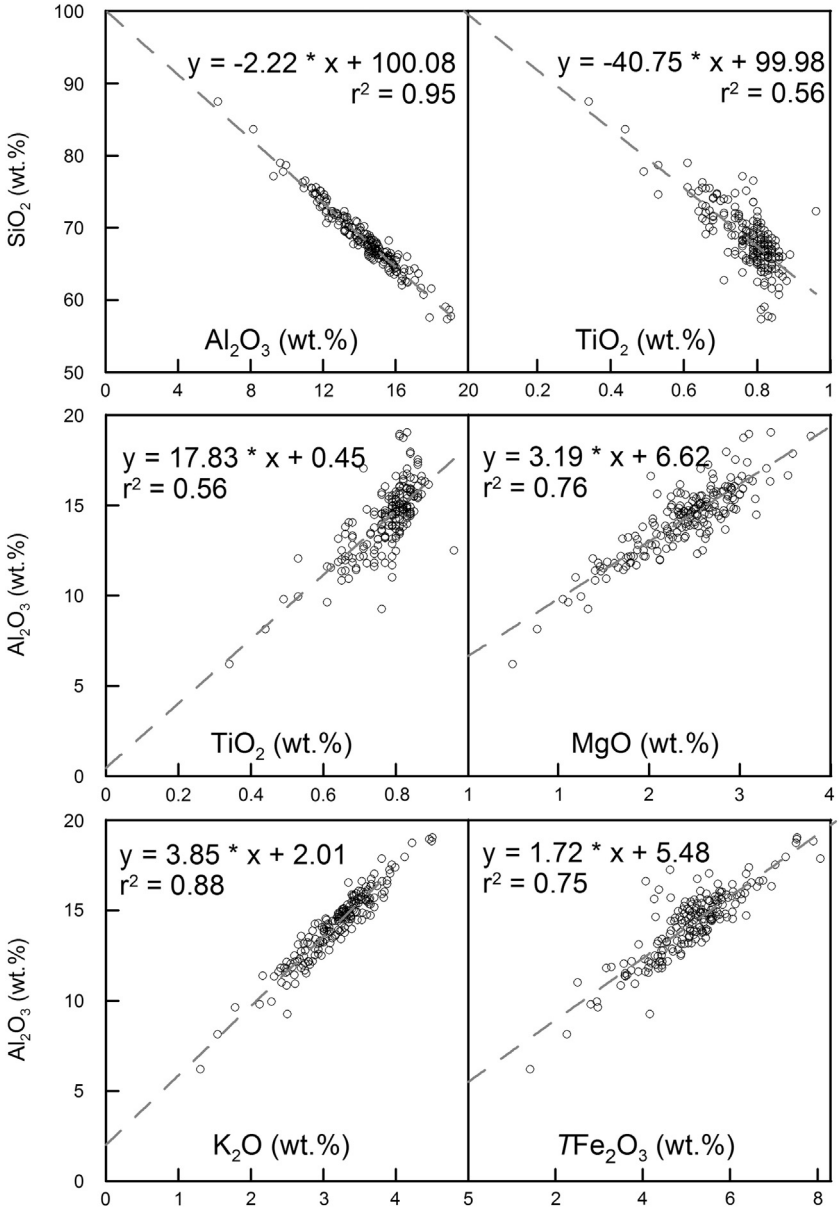

Fig. 4. Harker diagrams for 190 analyzed samples from the study section. Note that the immobile component plotted on the ordinate.

those concentrated in sand fractions (Fralick and Kronberg, 1997). In the study section (Fig. 4), we observe that the abundances of Al_2O_3 and TiO_2 fall on a line intercepting at 100% SiO_2, suggesting that the elements are immobile and concentrated into fine-grained fraction. The scattered distributions of TiO_2 abundances and the relatively low determination coefficients (r^2) of fit lines for TiO_2–SiO_2 and TiO_2–Al_2O_3 suggest that the behavior of Ti might be slightly different from Al. Therefore we regard Al as the only immobile element for further discussion.

On the plots of mobile-immobile pairs, the intercept of a regression line through the data on the ordinate will be positive if an element is enriched relative to an immobile component (Land et al., 1997). Plots of Mg, K and Fe against immobile Al show linear correlations with positive intercepts (Fig. 4). The patterns suggest that these elements have been enriched relative to Al, probably due to the lost of mobile Na and Ca.

5.2. Weathering history of the Kezilenuer section

Chemical weathering results in the removal of mobile elements and thus increases the sediment maturity, and the ultimate weathering products are generally quartz, clay, and oxides of aluminum. Quartz is the only chemically and physically durable constituent to be accumulated in great volume, allowing that its content is widely used as a maturity index (Pettijohn, 1954).

In contrast, feldspar group contains abundant mobile elements; consequently the dominant process during chemical weathering is the degradation of feldspars (Pettijohn, 1954). The ratio of immobile alumina to mobile alkalis, equals to $Al_2O_3/(Al_2O_3 + CaO + Na_2O + K_2O)$, namely CIA, is a good measure of the degree of weathering (Nesbitt and Young, 1982).

Most recently, Meunier et al. (2013) defined M^+–4Si–R^{2+} system, where M^+ sums the numbers of monocationic millimoles of alkaline and alkaline earth elements ($M^+ = Na^+ + K^+ + 2Ca^{2+}$), R^{2+} sums the numbers of divalent metallic elements ($R^{2+} = Mg^{2+} + Fe^{2+} + Mn^{2+}$), while 4Si represents the number of Si^{4+} divided by four. Using the novel M^+–4Si–R^{2+} ternary plot, they successfully incorporated SiO_2 content and metallic components into the weathering intensity scale (WIS), and defined a full weathering intensity scale to measure the difference between the compositions of unweathered and weathered samples. To a given sample, a WIS parameter, Δ4Si%, ranges from zero for the compositions of fresh rocks to 100 for the ultimate altered rocks (kaolinites).

Here we use the three approaches mentioned above to portray the weathering history of the study section (Fig. 5). The SiO_2 content, ranging from 57.4% to 87.5% with an average of 68.5 ± 4.4% (1 s.d.), shows a statistically weak but significant decreasing trend ($n = 190$, $r = 0.24$, $p = 0.001$). Relative to the upper continental crust, the WIS displays a decreasing trend similar to the SiO_2 content. These trends might suggest a long-term weakening of weathering of the Kezilenuer section during the late Oligocene and the Miocene.

Meanwhile, the CIA values from fine-grained rocks of the study section vary from 57.3 to 74.1, with an average of 66.8 ± 2.9. These low values are close to those of Pleistocene loess from western Pamir (Yang et al., 2006) and are higher than those of the detrital sediments in the present Taklamakan desert (Zhu and Yang, 2009). Different from other approaches, the CIA values are relatively stable before ~9 Ma, and decrease after ~9 Ma, probably indicating that the feldspars may have experienced comparable alteration during the interval from 30 to 9 Ma.

Bivariate plots of the oxides Al_2O_3, K_2O, CaO, Na_2O vs. CIA from the Kezilenuer section (Fig. 6) show that CIA negatively correlated with Na_2O and CaO, and positively correlated with Al_2O_3 and K_2O. These patterns further verify that the loss of Na_2O and CaO mainly contributes to the degree of chemical weathering of the sediments, i.e. the sediments are still in the early stage of the continental chemical weathering process and only plagioclase is being altered.

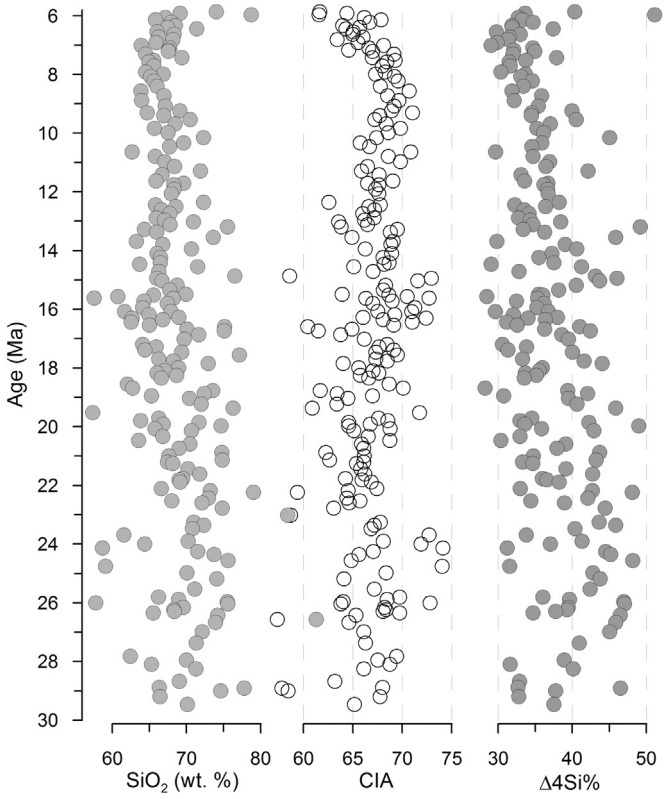

Fig. 5. Weathering indices as a function of age. CIA = $Al_2O_3/(Al_2O_3 + CaO + Na_2O + K_2O)$, where CaO represents the amount in silicate only (Nesbitt and Young, 1982). Δ4Si% is a full weathering intensity scale to measure the difference between the compositions of unweathered and weathered samples, 0 for fresh rocks and 100 for kaolinites (Meunier et al., 2013).

5.3. Sedimentary sorting

Many studies have investigated the role of sedimentary sorting and resulting grain size effects in obscuring the original signals of rock composition (Garzanti et al., 2009; Xiong et al., 2010; Yang et al., 2006). To minimize the potential impacts of grain size, we adopt the sampling strategy that all samples are collected from fine-grained beds on the site scale.

The principal effect of sedimentary sorting is a winnowing of phyllosilicate minerals from coarse-grained minerals (Argast and Donnelly, 1987; Taylor and McLennan, 1985). Consequently quartz and feldspar are preferentially concentrated into the coarse fraction, and phyllosilicate minerals into the finer-grained fractions. The ratios of oxides, such as SiO_2/Al_2O_3 and Na_2O/K_2O, hosted in the former and latter mineral groups are expected to increase from mudstone to sandstone, reflecting the decreasing proportions of phyllosilicates in sandstone (Ohta, 2004). Fig. 7 shows a bivariate plot of the element ratios sensitive to the sorting processes. Relative to the hypothetical differentiable sedimentary components (Argast and Donnelly, 1987), more than 90% of samples fall into a narrow interval and do not present a marked gradient. This pattern suggests that the sedimentary sorting is not an important determinant factor in controlling the geochemical composition of the study section, although the data distribute along a straight array and are somewhat proportional to the SiO_2 content.

5.4. Changes in provenance

5.4.1. Compositional variability of the section

As discussed above, aluminum is the most immobile element. We here use the abundance of alumina relative to the other major metallic

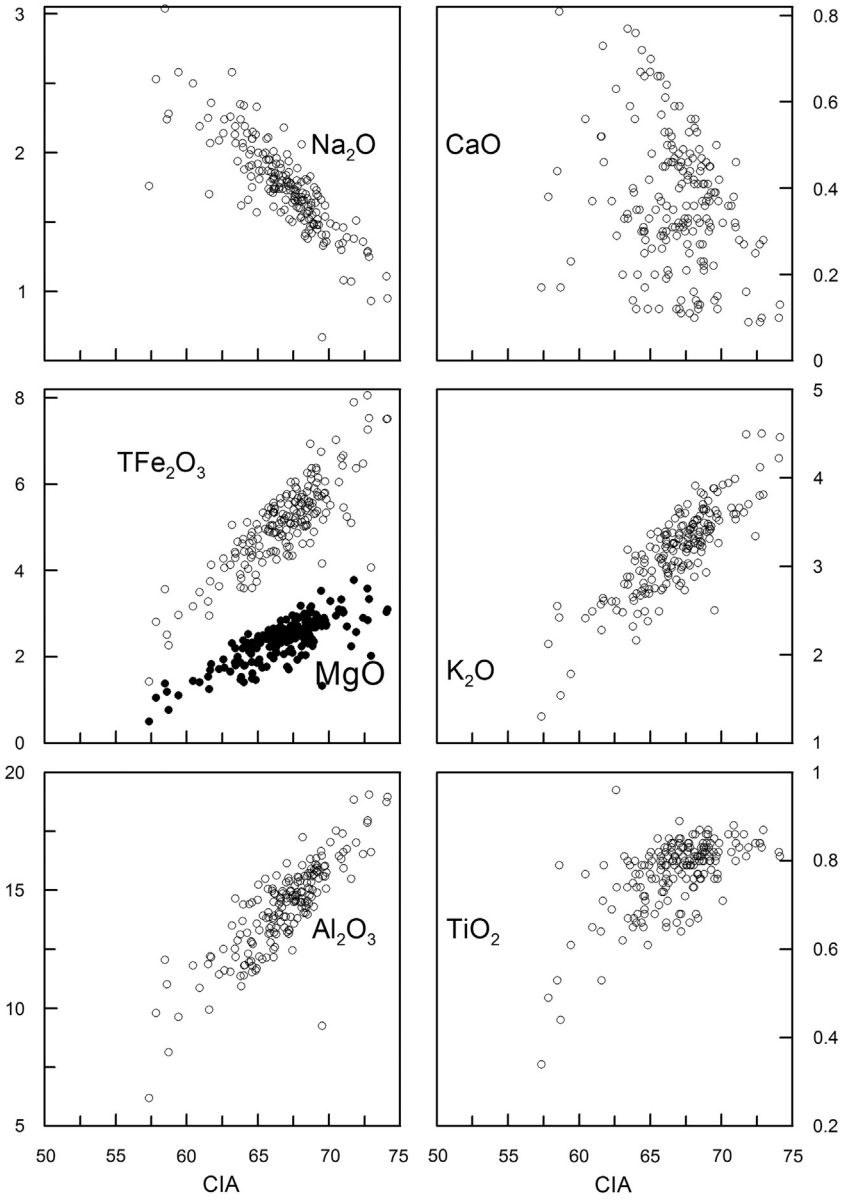

Fig. 6. Bivariate plots showing CIA and the abundance of oxides (wt.%).

cations to depict the variation of the bulk rock chemistry, following the index of compositional variability (ICV) defined by Cox et al. (1995): $ICV = (Fe_2O_3 + K_2O + Na_2O + CaO + MgO + MnO + TiO_2)/Al_2O_3$. Generally clay and nonclay silicate minerals have markedly different values for the ICV value. Clay minerals are enriched in aluminum; therefore they have a low ICV, commonly ranging from 0.03 to 0.78. In contrast, nonclay silicates contain a lower proportion of aluminum and the ICV tends to be higher.

Most ICV values from the study section exceed the range of values for common clay minerals and feldspars (0.54–0.87), except of several samples spanning 17–15 Ma (Fig. 8). The overall trend suggests that these samples contain abundant non-clay silicate minerals with high ICV values, roughly consistent with the weak weathering stage suggested by the weathering indices.

Different from the relatively stable CIA and WIS (Fig. 5), the ICV sequence can be grouped into three distinct stages, which are punctuated by two marked transitions. At ~23 Ma the ICV exhibits a rapid increase to the level well exceeding 1, and remains stable until ~17 Ma where it gradually goes back to 0.94 then stays relatively constant until the top of the section. Taking into account the weak influences of weathering and sorting processes, the observed ICV sequence would be dependent upon the changes in provenance.

Because the sum of the element components always maintains itself at 100%, the fluctuations in silica content may mask any subtle trends of other elements. To eliminate the effects of silica, we asterisked the oxides as their relative abundances out of the total analysis excluding SiO_2 (Fig. 8). Comparing to the raw data (Fig. 3), marked increases in the average abundance and in the variability are observed for the metallic elements through time, allowing better evaluations of the potential trends of the metallic elements.

The variations of oxides (Fig. 8) seem closely associated with the mobility of element. The highly mobile elements, such as Na, Ca, and Mg (Gaillardet et al., 2003), have larger variations than those of moderately mobile K and Mn, and that of most immobile Ti. Moreover, each oxide has smaller variation for samples from the upper part of the study section than those from the lower part, recalling that some essential changes occurred.

The increase in the ICV at ~23 Ma probably arises from the enhancement of MgO* and CaO* at the expense of Al_2O_3*, and the decrease in the ICV at ~17 Ma mainly arises from the decrease in Fe_2O_3* and the

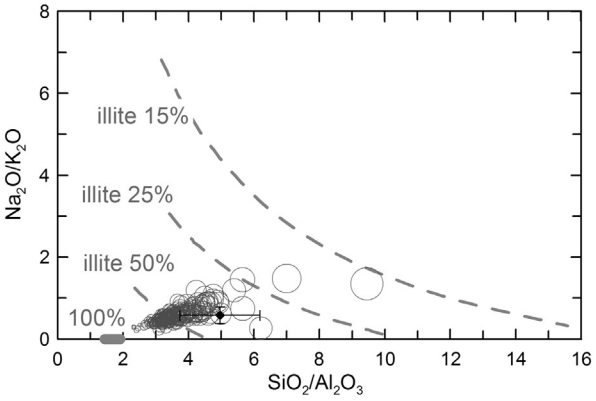

Fig. 7. Bivariate plot of element ratios sensitive to sedimentary sorting effects (Ohta, 2004) with symbol size proportional to SiO_2 content. Dashed lines are calculated contours for 15%, 25% and 50% illite compositions of the idealized differentiable sedimentary components (Argast and Donnelly, 1987).

increase in Al_2O_3*, as the other elements including MgO* and CaO* exhibit little changes. Relative to the immobile Al_2O_3*, the fundamental events in the geochemical sequence mainly involve the enhanced inputs of MgO and CaO at ~23 Ma and the reduced input of Fe_2O_3 at ~17 Ma from source rocks.

5.4.2. Constraints on the uplift of South Tian Shan

These changes in provenance may be generally attributed to reorganization of the sedimentary system by basement uplift, which provides an influx of nonclay silicate material. In the context of regional geology (Fig. 1), the material enriched Fe mainly comes for the igneous rocks along the late Paleozoic suture, and the source rocks enriched Mg and Ca would be the Harke Mountain, which contains the lower Paleozoic marble to the south of the suture. Considering that the Harke Mountain is the summit of the present South Tian Shan Mountains, a plausible scenario is that the uplift of the Harke Mountain initiated at ~23 Ma and the marble was exhumed and eroded, shedding the material enriched in Mg and Ca to the piedmonts where the study section was located. At ~17 Ma, the height of the uplifting Harke Mountain is sufficient to shelter Fe-enriched material from the suture to the Kuche Basin.

These speculations are supported by the detrital modes and heavy-mineral spectra of the sandstones from the study section. The contents of unstable lithic fragments, especially limeclasts, underwent a marked increase in Neogene (Li et al., 2006a). Further investigations into the geochemical composition of detrital garnets reveal that garnets in Cretaceous and Paleogene sandstones may well come from the low temperature and high pressure metamorphic rocks from the Southern Tian Shan Suture, while those in Neogene sandstone mainly come from meta-sedimentary rocks in the South Tian Shan (Li et al., 2007). Both lines of evidence from sandstone point to a large-scale uplift and consequent erosion in the South Tian Shan during the Neogene. Furthermore, on the scale of the Kuche Basin, unstable detrital heavy minerals, such as hornblende and pyroxene, increased since the Miocene, suggesting intensive tectonic uplift of the South Tian Shan during the Miocene (Li et al., 2004).

During the past twenty years extensive amount of low-temperature thermochronological studies has well acknowledged the building of the Tian Shan as a diachronous process in space, and the significant uplift occurred during the Neogene (Bullen et al., 2001, 2003; Chen et al., 2008; Du and Wang, 2007; Dumitru et al., 2001; Hendrix et al., 1994; Lü et al., 2013; Sobel et al., 2006; Sobel and Dumitru, 1997; Zhang et al., 2009). Apatite fission track analysis revealed that the central Tian Shan experienced a series of Paleogene and earlier cooling events, with only a few younger events that are widely recognized in the Tian Shan piedmonts (Du and Wang, 2007; Dumitru et al., 2001; Guo et al., 2006). For example, 25–20 Ma cooling event is widely recognized in

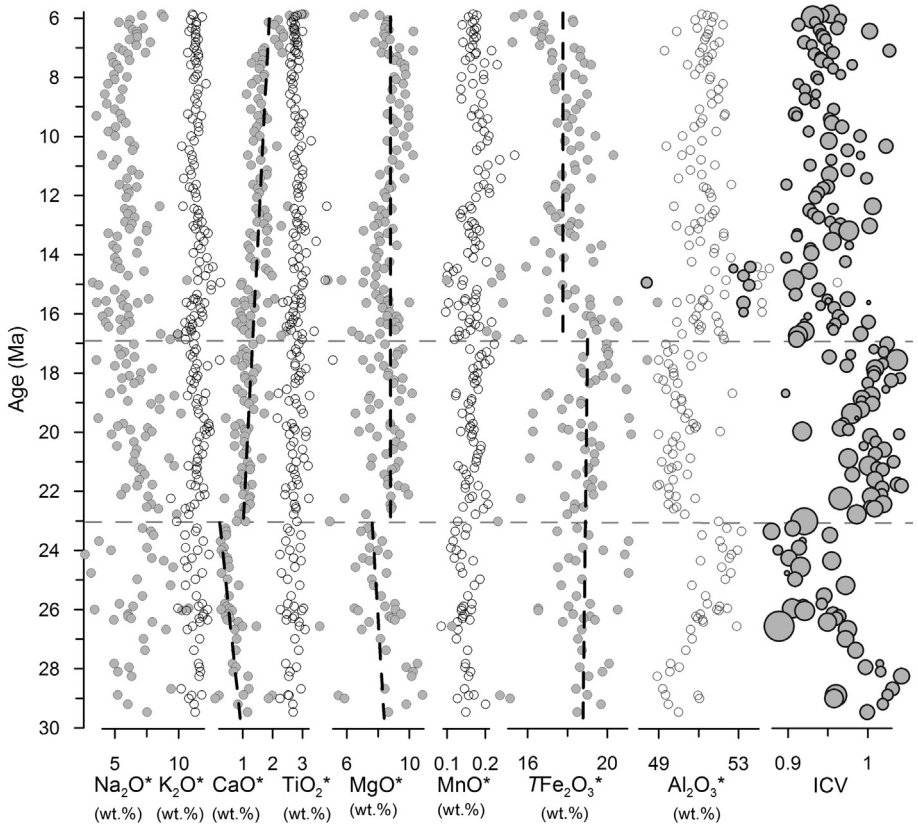

Fig. 8. Element abundance as a weight percentage of total analysis minus SiO_2 and the index of compositional variability (ICV) against age. ICV, as defined by Cox et al. (1995), equals to $(Fe_2O_3 + K_2O + Na_2O + CaO + MgO + MnO + TiO_2)/Al_2O_3$. Note that the circle size of ICV is proportional to SiO_2 content.

the piedmont of Kuche depression on the southern Tian Shan but not the intramontane Bayanbulak Basin to the north of the Kuche Basin, strongly implying that the uplifted region is mainly limited in the South Tian Shan Mountain (Du and Wang, 2007). These thermochronological observations supply a powerful support to our interpretations.

In addition, it is worth noticing that some elements show abrupt changes within the uppermost of the section. The relative concentrations of CaO and Na_2O show increase at ~7 Ma while Fe_2O_3 and MgO decrease in their abundances. Such increases of mobile elements are bound to decrease of the degree of weathering, as the CIA demonstrates (Fig. 5). Since these changes are accompanied by the acceleration of the sedimentation rate (Fig. 2), we attribute the weakening of weathering to the rapid accumulation of deposits, which somewhat refrains the leaching of mobile elements.

6. Conclusions

Within good chronostratigraphic framework, geochemical analyses of terrestrial sequences may track tectonic processes and climatic changes. We present a long-term and high-resolution primary element record in the Kuche depression, inner Eurasia, in order to understand the timing and magnitude of the tectonic uplift of the Tian Shan.

The Oligo-Miocene geochemical sequence from the Kuche depression is characterized by two irreversible shifts: increases of the concentrations of CaO and MgO at 23 Ma and decrease of the concentration of Fe_2O_3 at 17 Ma. These data further reveal a weak and stable weathering history and limited sorting effect, and thus we attribute the two fluctuations to provenance change dominantly. The early Miocene uplift of the South Tian Shan enhances non-clay silicate mineral influx to the Kuche depression since ~23 Ma and finally shelters the material from the iron-riched Central Tian Shan since ~17 Ma. This argument independently gainssupport from mineralogical variability on the study section and thermochronological results on the regional scale. Our study reveals the feasibility of conventional geochemical method on provenance change and tectonic uplift in such complex tectonic-sedimentary setting like the Tian Shan.

Supplementary data to this article can be found online at http://dx.doi.org/10.1016/j.palaeo.2016.01.020.

Acknowledgments

This work was financed by the National Basic Research Program of China (grant 2013CB956404), the Chinese Academy of Sciences key project (grant XDB03020503) and the NSFC (grant 41472151). We are grateful to the editor Prof. Thierry Corrège and three anonymous reviewers, whose constructive comments essentially improved the manuscript. We also thank Prof. Xiong Shangfa and Dr. Dong Xinxin for insightful discussions, Sun Dongjiang for field work and Guo Licheng for laboratory assistances.

References

Abdrakhmatov, K.Y., Aldazhanov, S.A., Hager, B.H., Hamburger, M.W., Herring, T.A., Kalabaev, K.B., Makarov, V.I., Molnar, P., Panasyuk, S.V., Prilepin, M.T., 1996. Relatively recent construction of the Tien Shan inferred from GPS measurements of present-day crustal deformation rates. Nature 384, 450–453. http://dx.doi.org/10.1038/384450a0.

Argast, S., Donnelly, T.W., 1987. The chemical discrimination of clastic sedimentary components. J. Sediment. Petrol. 57, 813–823.

Artyushkov, E.V., Hofmann, A.W., 1998. Neotectonic crustal uplift on the continents and its possible mechanisms. The case of Southern Africa. Surv. Geophys. 19, 369–415.

Avouac, J., Tapponnier, P., Bai, M., You, H., Wang, G., 1993. Active thrusting and folding along the northern Tien Shan and late Cenozoic rotation of the Tarim relative to Dzungaria and Kazakhstan. J. Geophys. Res. Solid Earth 98, 6755–6804. http://dx.doi.org/10.1029/92jb01963.

Bosboom, R., Dupont-Nivet, G., Grothe, A., Brinkhuis, H., Villa, G., Mandic, O., Stoica, M., Kouwenhoven, T., Huang, W., Yang, W., Guo, Z., 2014. Timing, cause and impact of the late Eocene stepwise sea retreat from the Tarim Basin (west China). Palaeogeogr. Palaeoclimatol. Palaeoecol. http://dx.doi.org/10.1016/j.palaeo.2014.03.035.

Bullen, M.E., Burbank, D.W., Gaver, J.I., Abdrakmatov, K.Y., 2001. Late Cenozoic tectonic evolution of the northwestern Tien Shan: new age estimates for the initiation of mountain building. GSA Bull. 113, 1544–1559. http://dx.doi.org/10.1130/0016-7606(2001)113<1544:LCTEOT>2.0.CO;2.

Bullen, M.E., Burbank, D.W., Garver, J.I., 2003. Building the Northern Tien Shan: integrated thermal, structural, and topographic constraints. J. Geol. 111, 149–165. http://dx.doi.org/10.1086/345840.

Charreau, J., Chen, Y., Gilder, S., Dominguez, S., Avouac, J.-P., Sen, S., Sun, D., Li, Y., Wang, W., 2005. Magnetostratigraphy and rock magnetism of the Neogene Kuitun He section (northern China): implication for Late Cenozoic uplift of the Tianshan Mountains. Earth Planet. Sci. Lett. 230, 177–192. http://dx.doi.org/10.1016/j.epsl.2004.11.002.

Charreau, J., Gilder, S., Chen, Y., Dominguez, S., Avouac, J.P., Sen, S., Jolivet, M., Li, Y., Wang, W., 2006. Magnetostratigraphy of the Yaha section, Tarim Basin (China): 11 Ma acceleration in erosion and uplift of the Tian Shan Mountains. Geology 34, 181–184. http://dx.doi.org/10.1130/G22106.1.

Charreau, J., Chen, Y., Gilder, S., Barrier, L., Dominguez, S., Augier, R., Sen, S., Avouac, J.-P., Gallaud, A., Graveleau, F., Wang, Q., 2009a. Neogene uplift of the Tianshan mountains observed in the magnetic record of the Jingou River section (Northwest China). Tectonics 28. http://dx.doi.org/10.1029/2007TC002137.

Charreau, J., Gumiaux, C., Avouac, J.-P., Augier, R., Chen, Y., Barrier, L., Gilder, S., Dominguez, S., Charles, N., Wang, Q., 2009b. The Neogene Xiyu Formation, a diachronous prograding gravel wedge at front of the Tianshan: climatic and tectonic implications. Earth Planet. Sci. Lett. 287, 298–310. http://dx.doi.org/10.1016/j.epsl.2009.07.035.

Chen, Z., Li, L., Liu, J., Gong, H., Jiang, R., Li, S., Zheng, E., Han, X., Li, X., Wang, C., Wang, G., Wang, G., Lu, K., 2008. Preliminary study on the uplifting-exhumation process of the western Tianshan Range, Northwestern China. Acta Petrol. Sin. 24, 625–636.

Christidis, G.E., 1998. Comparative study of the mobility of major and trace elements during alteratin of an andesite and a rhyolite to bentonite, in the islands of Milos and Kimolos, Aegean, Greece. Clay Clay Miner. 46, 379–399.

Cox, R., Lowe, D.R., Cullers, R.L., 1995. The influence of sediment recycling and basement composition on evolution of mudrock chemistry in the southwestern United States. Geochim. Cosmochim. Acta 59, 2919–2940.

Du, Z., Wang, Q., 2007. Mesozoic and Cenozoic uplifting history of the Tianshan region: insight from apatite fission track. Acta Geol. Sin. 81, 1081–1101.

Dumitru, T.A., Zhou, D., Chang, E.Z., Graham, S.A., Hendrix, M.S., Sobel, E.R., Carroll, A.R., 2001. Uplift, exhumation, and deformation in the Chinese Tian Shan. Geol. Soc. Am. Mem. 194, 71–99. http://dx.doi.org/10.1130/0-8137-1194-0.71.

Fralick, P.W., Kronberg, B.I., 1997. Geochemical discrimination of clastic sedimentary rock sources. Sediment. Geol. 113, 113–124.

Gaillardet, J., Viers, J., Dupré, B., 2003. Trace elements in river waters. In: Holland, H.D., Turekian, K.K. (Eds.), Treatise on Geochemistry. Elsevier, pp. 225–272.

Garzanti, E., Andò, S., Vezzoli, G., 2009. Grain-size dependence of sediment composition and environmental bias in provenance studies. Earth Planet. Sci. Lett. 277, 422–432. http://dx.doi.org/10.1016/j.epsl.2008.11.007.

Gresens, R.L., 1967. Composition–volume relationships of metasomatism. Chem. Geol. 2, 47–55.

Guo, Z., Zhang, Z., Wu, C., Fang, S., Zhang, R., 2006. The Mesozoic and Cenozoic exhumation history of Tianshan and comparative studies to the Junggar and Altai mountains. Acta Geol. Sin. 80, 1–15.

Han, B.-F., He, G.-Q., Wang, X.-C., Guo, Z.-J., 2011. Late Carboniferous collision between the Tarim and Kazakhstan–Yili terranes in the western segment of the South Tian Shan Orogen, Central Asia, and implications for the Northern Xinjiang, western China. Earth-Sci. Rev. 109, 74–93. http://dx.doi.org/10.1016/j.earscirev.2011.09.001.

Hao, Y., Su, X., Guo, X., Ding, X., 2000. Late Cretaceous calcareous nannofossils found from the Bashijike Formation in the Kuche Foreland, North Tarim Basin. Geoscience 14, 246–247.

Heermance, R.V., Chen, J., Burbank, D.W., Wang, C., 2007. Chronology and tectonic controls of Late Tertiary deposition in the southwestern Tian Shan foreland, NW China. Basin Res. 19, 599–632. http://dx.doi.org/10.1111/j.1365-2117.2007.00339.x.

Heermance, R.V., Chen, J., Burbank, D.W., Miao, J., 2008. Temporal constraints and pulsed Late Cenozoic deformation during the structural discription of the active Kashi foreland, northwest China. Tectonics 27. http://dx.doi.org/10.1029/2007TC002226.

Hendrix, M.S., Graham, S.A., Carroll, A.R., Sobel, E.R., McKnight, C.L., Schulein, B.J., Wang, Z., 1992. Sedimentary record and climatic implications of recurrent deformation in the Tian Shan: evidence from Mesozoic strata of the north Tarim, south Junggar, and Turpan basins, northwest China. Geol. Soc. Am. Bull. 104, 53–79. http://dx.doi.org/10.1130/0016-7606(1992)104<0053:SRACIO>2.3.CO;2.

Hendrix, M.S., Dumitru, T.A., Graham, S.A., 1994. Late Oligocene–early Miocene unroofing in the Chinese Tian Shan: an early effect of the India–Asia collision. Geology 22, 487–490. http://dx.doi.org/10.1130/0091-7613(1994)022<0487:LOEMUI>2.3.CO;2.

Huang, B., Piper, J., Peng, S., Liu, T., Li, Z., Wang, Q., Zhu, R., 2006. Magnetostragraphic study of the Kuche Depression, Tarim Basin, and Cenozoic uplift of the Tian Shan Range, Western China. Earth. Planet. Sci. Lett. 251, 346–364. http://dx.doi.org/10.1016/j.epsl.2006.09.020.

Jing, X.H., Shen, Z.Y., Wang, X., Yu, Y.L., Pan, X.Q., 2011. Magnetostratigraphic construct of Awate section in the north Tarim Basin: the impulse uplift of Tianshan Range. Chin. J. Geophys. — Chin. Ed. 54, 1575–1583. http://dx.doi.org/10.3969/j.issn.0001-5733.2011.06.017.

Lallier, F., Antonie, C., Charreau, J., Gaumon, G., Ruiu, J., 2013. Management of ambiguities in magnetostratigraphy correlation. Earth Planet. Sci. Lett. 371–372, 26–36. http://dx.doi.org/10.1016/j.epsl.2013.04.019.

Land, L.S., Mack, L.E., Milliken, K.L., Lynch, F.L., 1997. Burial diagenesis of argillaceous sediment, south Texas Gulf of Mexico sedimentry basin: a reexamination. Geol. Soc. Am. Bull. 109, 2–15.

Li, Y., 1984. The Tertiary System of China. Geological Publishing House, Beijing.

Li, Z., Wang, D., Lin, W., Wang, Q., 2004. Mesozoic–Cenozoic clastic composition in Kuqa depression, northwest China: implication for provenance types and tectonic attributes. Acta Petrol. Sin. 20, 655–666.
Li, S., Wang, Q., Li, Z., Wang, D., 2006a. Detrital modes of sandstones and their implications for basin-mountain evolution between the Kuqa depression and South Tian Shan Mountains. Chin. J. Geol. 41, 465–478.
Li, S.j., Zhang, R., Wang, Q., 2006b. Implications of the color of sediments and clay minerals for Tertiary cllimatic changes of Kuqa Depression. Acta Sedimentol. Sin. 24, 521–530.
Li, S., Shi, Y., Wang, Q., Li, Z., 2007. Changes of detrital heavy minerals' composition in the Kuqa depression from Cretaceous. Chin. J. Geol. 42, 709–721.
Li, C., Dupont-Nivet, G., Guo, Z., 2010. Magnetostratigraphy of the Northern Tian Shan foreland, Taxi He section, China. Basin Res. http://dx.doi.org/10.1111/j.1365-2117.2010.00475.x.
Lü, H., Wang, W., Chang, Y., Zhou, Z., 2013. Cenozoic episodic exhumation of the Tian Shan Range, NW China. Quat. Sci. 33, 812–822.
Lu, H., Wang, E., Meng, K., 2014. Paleomagnetism and anisotropy of magnetic susceptibility of the Tertiary Janggalsay section (southeast Tarim Basin): implications for Miocene tectonic evolution of the Altyn Tagh Range. Tectonophysics 618, 67–78. http://dx.doi.org/10.1016/j.tecto.2014.01.031.
Macaulay, E.A., Sobel, E., Mikolaichuk, A., Kohn, B., Stuart, F.M., 2014. Cenozoic deformation and exhumatio history of the Central Kyrgyz Tien Shan. Tectonics http://dx.doi.org/10.1002/2013TC003376.
MacLean, W.H., 1990. Mass change calculations in altered rock series. Mineral. Deposita 25, 44–49.
Métivier, F., Gaudemer, Y., 1997. Mass transfer between eastern Tien Shan and adjacent basins (central Asia): constraints on regional tectonics and topography. Geophys. J. Int. 128, 1–17. http://dx.doi.org/10.1111/j.1365-246X.1997.tb04068.x.
Meunier, A., Caner, L., Hubert, F., El Albani, A., Prêt, D., 2013. The weathering intensity scale (WIS): an alternative approach of the chemincal index of alteration (CIA). Am. J. Sci. 313, 113–143. http://dx.doi.org/10.2475/02.2013.03.
Molnar, P., Tapponnier, P., 1975. Cenozoic tectonics of Asia: effects of a continental collision. Science 189, 419–426.
Nesbitt, H.W., 2003. Petrogenesis of siliciclastic sediments and sedimentary rocks. In: Lentz, D.R. (Ed.), Geochemistry of Sediments and Sedimentary Rocks: Evolutionary Considerations to Mineral Deposit-forming Enviroments. Geological Association of Canada, GeoText, pp. 39–51.
Nesbitt, H.W., Young, G.M., 1982. Early Proterozoic climates and plate motions inferred from major element chemistry of lutites. Nature 299, 715–717. http://dx.doi.org/10.1038/299715a0.
Ogg, J.G., 2012. Geomagnetic polarity time scale. In: Grastein, F.M., Ogg, J.M., Schmitz, M.D., Ogg, G.M. (Eds.), The Geologic Time Scale 2012. Elsevier, Amsterdam, pp. 85–113.
Ohta, T., 2004. Geochemistry of Jurassic to earliest Cretaceous deposits in the Nagato Basin, SW Japan: implication of factor analysis to sorting effects and provenance signatures. Sediment. Geol. 171, 159–180. http://dx.doi.org/10.1016/j.sedgeo.2004.05.014.
Pettijohn, F.J., 1954. Classification of sandstones. J. Geol. 62, 360–365.
Sobel, E.R., Dumitru, T., 1997. Thrusting and exhumation around the margins of the western Tarim Basin during the India–Asia collision. J. Geophys. Res. Solid Earth 102, 5043–5063. http://dx.doi.org/10.1029/96JB03267.
Sobel, E.R., Chen, J., Heermance, R.V., 2006. Late Oligocene–Early Miocene initiation of shortening in the Southwestern Chinese Tian Shan: implications for Neogene shortening rate variations. Earth Planet. Sci. Lett. 247, 70–81. http://dx.doi.org/10.1016/j.epsl.2006.03.048.
Su, X., Guo, X., Ding, X., 2003. Late Cretaceous and Paleocene calcareous nannofossil assemblages from Kuche foreland basin in the northern Tarim Basin. Geoscience 17, 370–377.
Sun, J., Jiang, M., 2013. Eocene seawater retreat from the southwest Tarim Basin and implications for early Cenozoic tectonic evolution in the Pamir Plateau. Tectonophysics 588, 27–38. http://dx.doi.org/10.1016/j.tecto.2012.11.031.
Sun, J., Zhang, Z., 2009. Syntectonic growth strata and implications for late Cenozoic tectonic uplift in the northern Tian Shan, China. Tectonophysics 463, 60–68. http://dx.doi.org/10.1016/j.tecto.2008.09.008.
Sun, J., Li, Y., Zhang, Z., Fu, B., 2009. Magnetostratigraphic data on Neogene growth folding in the foreland basin of the southern Tianshan mountains. Geology 37, 1051–1054. http://dx.doi.org/10.1130/G30278A.1.
Tang, Z., Ding, Z., White, P.D., Dong, X., Ji, J., Jiang, H., Luo, P., Wang, X., 2011. Late Cenozoic central Asian drying inferred from a palynological record from the northern Tian Shan. Earth Planet. Sci. Lett. 302, 439–447. http://dx.doi.org/10.1016/j.epsl.2010.12.042.
Tang, Z., Huang, B., Dong, X., Ji, J., Ding, Z., 2012. Anisotropy of magnetic susceptibility of the Jingou River section: implications for late Cenozoic uplift of the Tian Shan. Geochem. Geophys. Geosyst. 13, Q03022. http://dx.doi.org/10.1029/2011gc003966.
Taylor, S.R., McLennan, S.M., 1985. The Continetal Crust: Its Composition and Evolution Balckwell.
Wack, M.R., Gilder, S.A., Maccauley, E.A., Sobel, E.R., 2014. Cenozoic magnetostratigraohy and magnetic properties of the southern Issyk-Kul basin, Kyrgyzstan. Tectonophysics http://dx.doi.org/10.1016/j.tecto.2014.03.030.
Windley, B.F., Allen, M.B., Zhang, C., Zhao, Z.Y., Wang, G.R., 1990. Paleozoic accretion and Cenozoic redeformation of the Chinese Tien Shan Range, Central Asia. Geology 18, 128–131. http://dx.doi.org/10.1130/0091-7613(1990)018<0128:PAACRO>2.3.CO;2.
Xiao, W., Windley, B., Sun, S., Li, J., Huang, B., Han, C., Yuan, C., Sun, M., Chen, H., 2015. A tale of amalgamation of three Permo-Triassic collage systems in Central Asia: oroclines, sutures, and terminal accretion. Annu. Rev. Earth Planet. Sci. 43, 477–507. http://dx.doi.org/10.1146/annurev-earth-060614-105254.
Xiong, S., Ding, Z., Zhu, Y., Zhou, R., Lu, H., 2010. A ~6 Ma chemical weathering history, the grain size dependence of chemical weathering intensity, and its implications for provenance change of the Chinese loess–red clay deposit. Quat. Sci. Rev. 29, 1911–1922. http://dx.doi.org/10.1016/j.quascirev.2010.04.009.
Yang, S., Ding, F., Ding, Z., 2006. Pleistocene chemical weathering history of Asian arid and semi-arid regions recorded in loess deposits of China and Tajikistan. Geochim. Cosmochim. Acta 70, 1695–1709. http://dx.doi.org/10.1016/j.gca.2005.12.012.
Yang, W., Dupont-Nivet, G., Jolivet, M., Guo, Z., Bougeois, L., Bosboom, R., Zhang, Z., Zhu, B., Heilbronn, G., 2015. Magnetostratigraphic record of the early evolution of the southwestern Tian Shan foreland basin (Ulugqat area), interactions with Pamir indentation and India–Asia collision. Tectonophysics 644–645, 122–137. http://dx.doi.org/10.1016/j.tecto.2015.01.003.
Yin, A., Nie, S., Craig, P., Harrison, T.M., Ryerson, F.J., Qian, X., Yang, G., 1998. Late Cenozoic tectonics evolution of the southern Chinese Tian Shan. Tectonics 17, 1–27. http://dx.doi.org/10.1029/97TC03140.
Zhang, Z., Zhu, W., Shu, L., 2009. Apatite fission track thermochronology of the Precambrian Aksu blueschist, NW China: implications for thermo-tectonic evolution of the north Tarim basement. Gondwana Res. 16, 182–188.
Zhang, T., Fang, X., Song, C., Appel, E., Wang, Y., 2014. Cenozoic tectonic deformation and uplift of the South Tian Shan: implications from magnetostratigraphy and balanced cross-section restoration of the Kuqa depression. Tectonophysics 628, 172–187. http://dx.doi.org/10.1016/j.tecto.2014.04.044.
Zhou, Z., Zhao, Z., Hu, Z., Chen, P., Zhang, S., Yong, Y., 2001. Statigraphy of the Tarmi Basin. Science Press, Beijing, p. 359.
Zhu, B., Yang, X., 2009. Chemical weathering of detrital sediments in the Taklamakan Desert, Northwestern China. Geogr. Res. 47, 57–70. http://dx.doi.org/10.1111/j.1745-5871.2008.00555.x.
Zhu, Y., Zhao, Y., Zhong, S., 2012. Palaeogene calcareous nannofossils from the Xiaokuzibai section of the Kuqa Depression, Tarim Basin. Acta Palaeontol. Sin. 51, 328–333.